Carbon dioxide photoelectron energy peaks at Mars

R.A. Frahm [a,*], J.D. Winningham [a], J.R. Sharber [a], J.R. Scherrer [a], S.J. Jeffers [a], A.J. Coates [b], D.R. Linder [b], D.O. Kataria [b], R. Lundin [c], S. Barabash [c], M. Holmström [c], H. Andersson [c], M. Yamauchi [c], A. Grigoriev [c], E. Kallio [d], T. Säles [d], P. Riihelä [d], W. Schmidt [d], H. Koskinen [d,e], J.U. Kozyra [f], J.G. Luhmann [g], E.C. Roelof [h], D.J. Williams [h], S. Livi [h], C.C. Curtis [i], K.C. Hsieh [i], B.R. Sandel [i], M. Grande [j], M. Carter [j], J.-A. Sauvaud [k], A. Fedorov [k], J.-J. Thocaven [k], S. McKenna-Lawler [l], S. Orsini [m], R. Cerulli-Irelli [m], M. Maggi [m], P. Wurz [n], P. Bochsler [n], N. Krupp [o], J. Woch [o], M. Fränz [o], K. Asamura [p], C. Dierker [q]

[a] *Southwest Research Institute, PO Drawer 28510, San Antonio, TX 78228-0510, USA*
[b] *Mullard Space Science Laboratory, University College London, Surrey RH5 6NT, UK*
[c] *Swedish Institute of Space Physics, Box 812, S-98 128 Kiruna, Sweden*
[d] *Finnish Meteorological Institute, Box 503, FIN-00101 Helsinki, Finland*
[e] *Department of Physical Sciences, University of Helsinki, P.O. Box 64, FIN-00014 Helsinki, Finland*
[f] *Space Physics Research Laboratory, University of Michigan, Ann Arbor, MI 48109-2143, USA*
[g] *Space Science Laboratory, University of California in Berkeley, Berkeley, CA 94720-7450, USA*
[h] *Applied Physics Laboratory, Johns Hopkins University, Laurel, MD 20723-6099, USA*
[i] *University of Arizona, Tucson, AZ 85721, USA*
[j] *Rutherford Appleton Laboratory, Chilton, Didcot, Oxfordshire OX11 0QX, UK*
[k] *Centre d'Etude Spatiale des Rayonnements, BP-4346, F-31028 Toulouse, France*
[l] *Space Technology Ireland, National University of Ireland, Maynooth, Co. Kildare, Ireland*
[m] *Istituto di Fisica dello Spazio Interplanetari, I-00133 Rome, Italy*
[n] *Physikalisches Institut, University of Bern, CH-3012 Bern, Switzerland*
[o] *Max-Planck-Institut für Aeronomie, D-37191 Katlenburg-Lindau, Germany*
[p] *Institute of Space and Astronautical Science, 3-1-1 Yoshinodai, Sagamichara, Japan*
[q] *Technical University of Braunschweig, Hans-Sommer-Strasse 66, D-38106 Braunschweig, Germany*

Abstract

The ELectron Spectrometer (ELS) from the Analyzer of Space Plasmas and Energetic Atoms (ASPERA-3) flown on the Mars Express spacecraft has an 8% energy resolution, combined with the capability to oversample the martian electron distribution. This makes possible the resolution and identification of electrons generated as a result of the He 304 Å ionization of CO_2 at the martian exobase on the dayside of the planet. Ionospheric photoelectrons were observed during almost every pass into the ionosphere and CO_2 photoelectron peaks were identified near the terminator. Atmospherically generated CO_2 photoelectrons are also observed at 10,000 km altitude in the martian tail near the inner magnetospheric boundary. Observations over a wide range of spacecraft orbits showed a consistent presence of photoelectrons at locations along the inner magnetospheric boundary and in the ionosphere, from an altitude of 250 to 10,000 km.
© 2006 Elsevier Inc. All rights reserved.

Keywords: Mars; Ionospheres; Atmospheres; Magnetospheres

1. Introduction

The European Space Agency (ESA) Mars Express spacecraft (launched June 2, 2003) reached Mars and was injected

---

there into orbit on December 25, 2003. One of the Mars Express investigations is the study of the solar wind–planet interaction, which is conducted by the Analyzer of Space Plasmas and Energetic Atoms-3 (ASPERA-3) experiment (Barabash et al., 2004). ASPERA-3 has been measuring ions, electrons, and Energetic Neutral Atoms (ENAs) since arrival at Mars. The Electron Spectrometer (ELS) is one of the instruments of the ASPERA-3 experiment.

Prior to launch of the Mars Express spacecraft, it was known that the ionospheric spectrum contains photoelectron energy peaks from atmospheric gasses as does any other planetary atmosphere. The major photoelectron energy peaks in the range 21–24 eV and at 27 eV result from both O and CO_2 ionization with the majority of electrons generated from CO_2 ionizations near the exobase. The ELS was designed to measure these photoelectron energy peaks. Using its high energy resolution modes to probe the high-altitude ionosphere, ELS obtains an electron spectrum. ELS is the first high resolution ($\Delta E/E = 8\%$) instrument to measure photoelectron energy spectra at a planet other than Earth.

In addition to the predicted major photoelectron energy peaks observed in the martian ionosphere, ELS observes the same major photoelectron energy peaks in the distant tail of Mars. The observations show that the electron flow in the energy region where the CO_2 photoelectron peaks dominate the energy spectrum is directed away from the planet, suggesting an outward flow of these electrons from Mars.

2. Background

In general, photoelectrons are generated by ionization of planetary atmospheres by solar photons. These solar photons can come from either the solar continuum or discrete solar lines. Photoelectrons also can cause impact ionization which has the effect of smoothing the photoelectron spectrum. The degree of smoothness is determined by the degree of transparency of the region to electron transport.

The electron spectrum in the martian ionosphere is dominated by signatures from CO_2. CO_2 is ionized by photons of wavelength less than 898.5 Å. At 304 Å, an intense solar helium line exists which causes ionization of the CO_2 molecule in the martian atmosphere, creating a ground state CO_2^+ and generating a 27 eV electron. Additional electrons are generated through the ionization of CO_2 by a He 304 Å photon. Again, the final state is CO_2^+; however, the CO_2^+ is not in the ground state. Since the additional states of CO_2^+ absorb specific quanta of energy, the ejected electrons are produced with their characteristic energies in the 21–24 eV energy range. These are major peaks which dominate the less than 60 eV electron spectrum and which ELS was designed to resolve.

The electron spectrum in the martian ionosphere below 100 eV was calculated by Mantas and Hanson (1979) based on an electron spectrum inferred from altitude profiles of Ar, Ne, CO_2, CO, O_2, O, NO, and N_2 measured during the decent of the Viking 1 lander. Using the most up-to-date atomic cross-section data available at that time, they calculated the photoelectron spectrum for two magnetic field conditions: hor-

izontal field and vertical field. They suggested that the horizontal field calculations would be appropriate at the equator of Mars while the vertical field calculations would be appropriate at the poles. However, the vertical field calculations are more appropriate between the crustal magnetic anomalies where the remanent magnetic field has mostly a radial component. These magnetic anomalies at Mars were observed by the Mars Global Surveyor (MGS) Magnetometer (MAG) and are described by Connerney et al. (2001). These magnetic anomalies are independent localized magnetic bubbles which are distributed more in the southern hemisphere than in the northern hemisphere and aid in standing off the solar wind.

Fox and Dalgarno (1979) reached similar conclusions to those of Mantas and Hanson without the inclusion of a magnetic field in their model. The atomic cross-sections used by Fox and Dalgarno, and Mantas and Hanson were similar. Neither theory included production from Auger electrons.

Photoelectrons within the energy range between 21 and 24 eV and at 27 eV could be generated by carbon dioxide or atomic oxygen ionization. The ionization potentials in this region are nearly equal, at 13.77 eV ($X^2\Pi_g$), 17.32 eV ($A^2\Pi_u$), and 18.10 eV ($B^2\Sigma_u^+$) for CO_2 and 13.62 eV (^4S), 17.10 eV (^2D), and 18.50 eV (^2P) for O (Mantas and Hanson, 1979). At Mars, Fox and Dalgarno report that a detailed analysis shows that vertical column photoionization rate for CO_2 is about 11 times that of O for ionization potentials near 13 eV, about 5 times near 17 eV, and 9 times near 18 eV. Thus, the majority of photoelectrons measured at Mars between 21 and 24 eV and at 27 eV are due to CO_2 ionization. Electron impact ionization may modify these numbers slightly, but the electron impact process removes ionization energy from the kinetic energy of the electron, creating an energy cascading process which acts to smooth out the electron energy spectrum. There is a much smaller probability that the energy of the electron or secondary electron will obtain the peak energies described in this paper.

The martian ionospheric photoelectrons have been observed by the MGS Electron Reflectometer (ER). Mitchell et al. (2001) recorded elevated electron flux in the ER energy band corresponding to the Mantas and Hanson (1979) and Fox and Dalgarno (1979) calculations. However, the ER energy resolution of $\Delta E/E = 25\%$ was too coarse to resolve the structure of these photoelectron peaks.

Atmospheric photoelectrons are generated near the exobase, defined as the level at which the atmospheric scale height and the collisional mean free path are equal. Thus, the exobase is the point above which the electron gas becomes free to expand and is not collisionally bound. This is estimated from Mantas and Hanson (1979) as between 130 and 150 km where they show vertical transport becoming important. Their results show that the photoelectron flux is decreased by about a factor of 2 at energies of 40 eV and below if the magnetic field is in the vertical direction as opposed to the horizontal direction. However, in their vertical magnetic field model, photoelectrons are allowed to escape from the topside of the martian atmosphere. Since MGS MAG found many structures in the crustal magnetic field, it is likely that the photoelectron flux lies somewhere between the two magnetic field configurations modeled and dis-

cussed by Mantas and Hanson. Thus, photoelectrons generated near the exobase are most likely transported along the magnetic field line, either to escape the atmosphere or to become trapped within the magnetic field.

3. Instrument

The ELS is a spherical top hat which samples electrons from a 360° × 4° wide field of view (FOV). The 360° of azimuth are divided into 16 sectors, each 22.5° wide. The ELS *k*-factor (or energy sensitivity) and resolution (Sablik et al., 1990) are slightly sector-dependent, and the average values are 7.23 ± 0.05 eV/V and 0.083 ± 0.003 ($\Delta E/E$), respectively. The ELS *k*-factor and resolution were determined at 10 keV by laboratory measurements. Deviations of the *k*-factor and resolution with input electron energy were folded into an energy-dependent relative microchannel plate (MCP) efficiency factor. The energy-independent physical geometric factor is 5.88×10^{-4} cm^2 sr.

ELS covers the energy range from 1 eV to 20 keV which is influenced by spacecraft charging (see below). This is accomplished using a dual range deflection power supply, referred to as the low range and high range. Each power range has a control resolution of 4096 states within its full scale. The voltage ranges are 0 to 20.99 V (to measure up to about 130 eV) for the low range and 0 to 2800.0 V (to measure up to about 20 keV) for the high range (energy conversion is sector-dependent). Of the 8192 possible deflection voltage values, 128 may be selected to form an energy sweep. Accumulation of electrons for each step takes 28.125 ms, with an additional 3.125 ms of dead time between each step. The total sweep (128 steps) is completed in 4 s. The energy sweep is a controlled decay from its highest programmed voltage to its lowest, with the last step of the sweep used as a flyback step to reset the sweep.

For most of the data, ELS was in a survey mode in which the energy was swept logarithmically with an 8% spacing from about 0.6 eV to about 20 keV. The ELS protection grid was typically set to −5 V during survey mode (this value will not be constant throughout the mission). For some of the data presented in this paper, ELS stepped energies linearly, from about 1 eV to about 127 eV in 1 eV increments. The ELS protection grid is typically set to spacecraft ground during linear stepping. In this mode, undersampling conditions occur when detecting electrons below 13 eV and oversampling conditions occur when detecting electrons above that value. Oversampling produces an effective variable-width resolution that is higher than that of an individual sample. ELS is mounted on the ASPERA-3 scan platform. In the case of the data presented in this paper, the scanner remained parked in its launch position.

In the launch position of the scanner, the top hat plane of ELS is parallel to the spacecraft *X*–*Z* plane. Attitude angles are defined in a clockwise fashion from the spacecraft +*Z*-axis toward the spacecraft +*X*-axis. In the launch position, viewing angles for each ELS sector are given in Table 1. The spacecraft +*Z*-axis pointing direction varies throughout the orbit and does not consistently point in the same direction orbit-to-orbit. ELS

Table 1
ELS launch viewing angles

ELS sector	Viewing angle center (°)	ELS sector	Viewing angle center (°)
0	191.25	8	11.25
1	213.75	9	33.75
2	236.25	10	56.25
3	258.75	11	78.75
4	281.25	12	101.25
5	303.75	13	123.75
6	326.25	14	146.25
7	348.75	15	168.75

sector numbers are used throughout this paper to denote azimuth angle orientation.

It is worth noting that in the current position of the ASPERA-3 scan platform, ELS sector 12 looks partly across the spacecraft. ELS sector 13 also looks across the spacecraft, but the connecting arm of the solar array lies within its field of view. ELS sectors 14 and 15 view across most of the spacecraft. ELS sector 0 also looks partly across the spacecraft, and the spacecraft sun sensor protrudes into its field of view.

Spacecraft charging affects the electron energy by adding an energy offset. The Mars Express (MEX) spacecraft does not include instrumentation to independently determine spacecraft charge. MEX spacecraft charge is inferred by two types of electron signatures and fails if neither exists in the ELS data. The first occurs when the spacecraft is charged positively. A positive spacecraft potential is inferred when a flux peak is exhibited in the electron energy spectrum at identical energies for all measurement angles (Johnstone et al., 1997). When the MEX is in the martian magnetosheath, variable positive charging is observed (limited by the protection screen bias) up to about +10 V (it is usually less than +8 V). The second occurs when the spacecraft is charged negatively. A negative spacecraft potential is observed at all measurement angles as a shift in the CO_2 photoelectron energy peaks location from their theoretical value. When photoelectrons are present in the ionosphere, the inferred spacecraft potential is always negative, is variable, and has been observed up to −10 V, although it is usually within the −4 to −8 V range. It is worthy to note that when MEX is in the martian tail, the charge on the MEX spacecraft is determined by either the above two methods, and has been observed to be both positive and negative (ranging between −10 and +10 V). The rate of change of spacecraft charging within the martian tail can be several volts within seconds; whereas, charging values within the magnetosheath and ionosphere slowly drift on the order of minutes for the same amount of change. No matter the location of the spacecraft, if neither of these two types of electron signature exists, no spacecraft potential can be inferred, as typical in the solar wind or Mars shadow with MEX. Electron spectra presented in this paper are not adjusted for spacecraft charging.

4. Observations

It was expected that the ELS would record the major photoelectron peaks in the martian ionosphere, and these were indeed

observed. On June 7, 2004 (day 159) the MEX spacecraft (orbit 484) entered the Mars ionosphere on the nightside of the planet (Fig. 1). MEX reached pericenter at 06:39:10 UT while in darkness. After pericenter, the MEX spacecraft experienced sunrise and detected atmospheric photoelectrons. After photoelectron detection, MEX continued through the IMB, magnetosheath, and bow shock to the upstream solar wind.

Fig. 2 shows ELS data displayed as energy–time spectrograms of the differential electron energy intensity (erg/ $(cm^2 s\, sr\, eV)$) taken in the dayside ionosphere on June 7, 2004 (day 159) for four of the 16 ELS sectors. At this time, ELS sector 4 looked up, away from the planet measuring electron flow traveling toward Mars and sector 12 looked down, toward the planet measuring electron flow traveling away from Mars, with sector 0 viewing toward noon (electrons flowing from noon) and 8 viewing toward dawn (electrons flowing from dawn). Between 06:40 and 06:50 UT, ELS observed ionospheric plasma. While observing ionospheric plasma, ELS records the major photoelectron energy peaks from CO_2 which are generated near the martian exobase and transported to the observation point. In the ionosphere, the photoelectron peaks are observed in every ELS sector.

A subset of 15 spectra from Fig. 2 between 06:48 and 06:49 UT have been averaged and displayed in Fig. 3. Spectra showing electron flow toward and away from Mars (sectors 4 and 12) are given in differential energy intensity. The major photoelectron peaks are seen to occur at energies lower than was predicted by theory. Observations over many passes indicate that the Mars Express spacecraft charges negatively by several volts when in the martian ionosphere and charges positively by several volts in the sunlit magnetosheath. The level of spacecraft charging varies. As discussed earlier, the Mars Express spacecraft has no means whereby spacecraft charging can be directly measured. The theoretical energies of the major photoelectron peaks are assumed to mark their spectral positions. With this assumption, it can be deduced that the Mars Express spacecraft charged to a value of approximately −7 V at the time of the spectra shown in Fig. 3.

Fig. 4 shows the integrated flux between 13.5 and 21.5 eV as a function of look direction for each of the sectors of ELS (sector numbers are marked on these data for reference as well as the electron flow direction). Slight variations were probably due to inhomogeneities in the plasma. Since the Mars Express spacecraft has no magnetometer; the exact pitch angle for each ELS sector cannot be determined by direct measurement. However, the Mars Global Surveyor magnetometer data was used by Cain et al. (2003) to generate a model of the Mars magnetic field in the ionosphere. This model may be used to estimate the pitch angle of each ELS sector for the ELS data shown in Fig. 4 (in order to get an idea of the range of pitch angles measured) and is with respect to the modeled magnetic field. These results are shown in Fig. 5, where the locations of the center of each ELS anode have been marked, corresponding to those shown in Fig. 4. The average pitch angle of each detector pair is also shown (red) in Fig. 5 for reference. For this spacecraft orientation, ELS sampled plasma over a wide range of pitch angles. Larger numbered ELS sectors measured greater fluxes, with the

exception of the ELS sectors viewing across the spacecraft (sectors 13, 14, 15, and 0).

Although the Cain et al. (2003) model is to our knowledge the best to date for describing the martian crustal magnetic field, its authors point out that more scatter is obtained in the horizontal field values of the dayside (as opposed to nightside) MGS data. This suggests the influence of external fields preferentially on the dayside, likely associated with currents resulting from the interaction of the solar wind and the martian atmosphere and ionosphere. These effects will result in uncertainties in our determination of pitch angle. If we simply compare measured and modeled fields shown by Cain et al., we obtain a "nominal" uncertainty in pitch angle of about 15°. However, the Cain et al. model is based primarily on dayside observations restricted to low-altitudes ($< \sim$200 km) and nightside (shadowed by the planet) observations, both of which will reduce the influence of ionospheric sources. Thus, in specific instances, use of the model to calculate pitch angle could result in uncertainties larger than the stated 15°. The actual value will of course depend on the strength and direction of the external field sources.

The example of Fig. 2 shows CO_2 photoelectron peaks at altitudes below about 630 km. They were produced near the sunlit exobase, and the peaks were sharp and easily resolved. Other examples in the ELS data show that photoelectrons were also observed at higher altitudes as Mars Express passed through the region just beneath the boundary of the magnetosheath. This boundary has been referred to as the induced magnetosphere boundary (IMB) by Lundin et al. (2004) and is the envelope of the induced martian magnetosphere identified by its plasma signature, the boundary below which the dominant plasma is planetary in origin. The IMB is located at or near the magnetic pile-up boundary (MPB) defined by MGS. The difference between the MBP and IMB is that the MPB is defined using the magnetic field signature and the IMB is defined using the particle signature. Other common names which have been used to describe this region are the planetopause and ion composition boundary. At and below the IMB, the shape of the boundary as well as the behavior of the interior plasma is influenced by the crustal fields of Mars (Brain et al., 2003).

High-altitude photoelectrons (identified by their characteristic CO_2 peaks) were seen at various local times and at altitudes up to several thousand kilometers. In one case (April 24, 2004, at 07:00:02 UT, with a planetodetic altitude of 7107.4 km, a solar zenith angle of 146.9°, a planetocentric latitude of 13.15°, and a planetocentric longitude of 242.65°), the CO_2 peaks were simultaneously observed flowing toward and away from the planet. The CO_2 peaks flowing toward the planet were less intense, less well defined, and appeared at a slightly lower energy indicating that they had undergone more energy cascading during their travel in contrast to those CO_2 peaks flowing away from the planet. Although peak observations are persistent, we point out that the photoelectrons were not observed at every IMB crossing. Whether or not they were observed at a given location is expected to depend critically on the geometry and path through the atmosphere of the magnetic field line at ELS. Further study in this regard is reported by Liemohn et al. (2006).
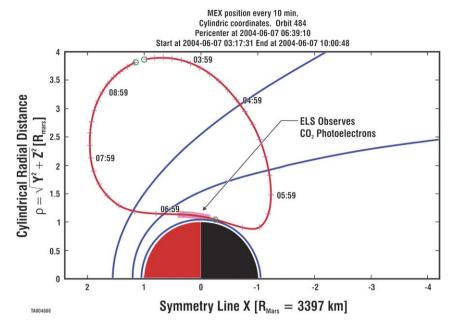
Fig. 1. Mars Express orbit 484 on June 7, 2004. As Mars Express traveled through the ionosphere, it achieved pericenter on the nightside of Mars. Mars Express gained altitude on the Mars dayside, crossing the IMB, magnetosheath, and bow shock on the dayside of the planet. Mars cylindrical coordinates are used to express the spacecraft orbit as distance from the Mars–Sun line. The two blue curves mark the average positions of the bow shock and MPB as calculated by Vignes et al. (2000).
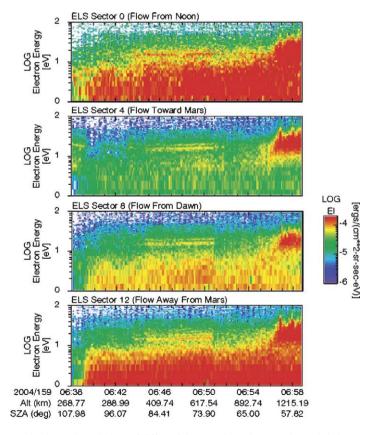

Fig. 2. Energy–time spectrogram in the martian ionosphere. Values of differential energy intensity are color coded. Spectrograms are marked in terms of electron flow and show photoelectron peaks measured in selected directions. Spacecraft location is given in terms of planetodetic altitude (Alt), solar zenith angle at the spacecraft (SZA), planetocentric latitude (PcLat), and planetocentric longitude (PcLon), which is measured toward the east.

On January 9, 2005 (Fig. 6), the MEX orbit (1256/1257) allowed the spacecraft to sample plasma deeper in the tail than in the previous case. At about 13:00 UT, the continuous magnetosheath plasma signature was interrupted and plasma turbulence was observed at magnetosheath energies until 13:32 UT when photoelectrons were observed. (Note that while mea-
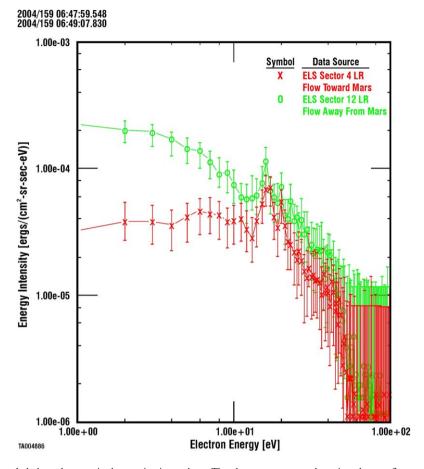
Fig. 3. Energy spectra of oversampled photoelectrons in the martian ionosphere. The electron spectrum observing electron flow toward Mars (red sector 4) and the spectrum observing electron flow away from Mars (green sector 12) indicate that the photoelectron peaks are observed in simultaneous spectra, flowing both away and toward the planet. Error bars indicate average error values for 1 min and include Poisson statistics, instrument error, and telemetry compression error. Here, the solar latitude is $-38.2°$, solar time is 7.05 h, solar zenith angle is 77.9°, planetocentric longitude is 100.2°, planetocentric latitude is $-46.5°$, planetodetic latitude is $-47.4°$, and the planetodetic altitude is 526 km.
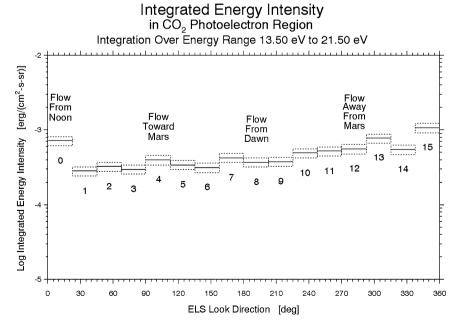

Fig. 4. ELS look directions of martian ionospheric photoelectron intensities. ELS look directions around its viewing plane are shown as an integral of differential energy intensity including only the energy region of the CO_2 photoelectron peaks. Error boxes indicate the projected integration error. Positions of ELS sector numbers are shown below the data and above the data are marked the electron flow directions.

Integrated Energy Intensity
in CO_2 Photoelectron Region
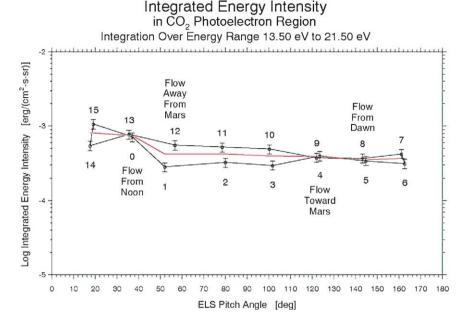Integration Over Energy Range 13.50 eV to 21.50 eV

Fig. 5. Approximate pitch angle variation of martian ionospheric photoelectrons. Integral data from Fig. 4 has been remapped using a magnetic field model to give an approximate indication of the pitch angle range covered by ELS at this time. ELS sector numbers and electron flow directions are given in correspondence with Fig. 4.
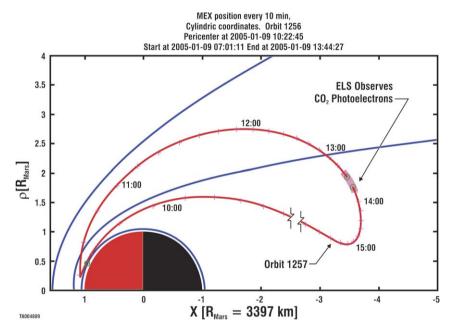
Fig. 6. Mars Express orbit 1256 on January 9, 2005. As Mars Express traveled through the magnetosheath, crossing the IMB where turbulent plasma was detected. Photoelectrons were detected equatorward of the IMB. Mars Express orbit number changed to 1257 during detection of photoelectrons. This plot has a similar format to that shown in Fig. 1.

suring photoelectrons, the MEX orbit changes from 1256 to 1257.)

Photoelectrons observed at apoapsis on January 9, 2005 are shown in Fig. 7 in energy–time spectrogram format. Again, four of the 16 ELS sectors are shown. At this time, ELS sector 3 looked toward the planet measuring electron flow away from Mars and sector 11 looked toward the tail measuring electron flow traveling toward Mars, with sectors 7 and 15 viewing approximately perpendicular to the average IMB location. Be-

tween 13:32 and 13:53 UT, ELS observed photoelectron plasma coming from the planet (observed here in sector 3). The data shown in this example were taken in a survey mode when ELS was not being oversampled. In this survey mode, the ELS protection grid is active and repelled electrons with energies less than 5 eV.

The CO_2 photoelectrons observed in the martian tail were not observed at all angles. They were observed flowing toward and away from the planet, with greater intensity flowing away

from the planet. (In fact, we have never observed the photoelectrons to flow in the perpendicular to the IMB.) These observations suggest that the flow is along the local field line, which is expected to be approximately aligned with the IMB surface. (Using the model field to calculate pitch angles at this location would clearly be unreliable.) The energy spectra shown in Fig. 8 for electrons flowing away from the planet (shown in red) and those flowing toward the planet (green) are averaged between 13:43:25 and 13:44:32 UT to improve statistics and to highlight the average spectral shape differences. CO_2 peaks are easily seen between 13 and 21 eV. Again, assuming the photoelectron peaks had not degraded in energy and the theoretical energy was appropriate to judge spacecraft charging, the spacecraft was charged to approximately −9 V at this time.

Fig. 9 shows the integrated flux between 12.9 and 20.9 eV as a function of look direction for each of the ELS sectors (sector numbers and flow directions are indicated for reference) in the same format as Fig. 4. The orientation of the spacecraft is such that higher fluxes are measured by ELS sector 13 (looks at the base of a solar array), sectors 14, 15, and part of sector 12 (viewed across the spacecraft), and sector 0 (looks at the solar sensor). Disregarding these sectors a showing possible contamination from the spacecraft, the variation in flux was found to be is sinusoidal with the peaks values toward and away from the planet. This is indicative of an electron distribution aligned along the local magnetic field line with fluxes along the field line exceeding those perpendicular by at least a factor of two.

5. Discussion

ELS is the first electron spectrometer to resolve the major photoelectron energy peaks generated from UV ionization of the martian atmosphere. The data presented show these peaks at altitudes between 400 and 10,000 km. However, these peaks were observed over the full range of altitude between and down to 250 km altitude (i.e., over the full range of spacecraft altitudes).

As indicated in both Mantas and Hanson (1979) and Fox and Dalgarno (1979), most of the photoionization at low altitudes of around 130 km is produced from photoionization of carbon dioxide. As a function of altitude, the photoelectron production rate decreases by several orders of magnitude by an altitude of about 200 km where the majority of photoelectron production comes from atomic oxygen ionization. Both Fox and Dalgarno (1979) and Krasnopolsky and Gladstone (1996) indicate that both the oxygen and carbon dioxide densities continue to decrease exponentially in the martian exosphere, indicating that the photoionization production rate continues to exponentially decrease with increasing altitude. Mantas and Hanson (1979) show that photoelectron transport is significant above 145 km leading to nearly constant photoelectron flux at specific energies by altitudes of 300 km (with a magnitude of about half of the photoelectron flux at 145 km). ELS measurements indicate that the photoelectron flux measured at about 600 km is nearly the same or less than the photoelectron flux measured at about 270 km (zero in the case where the solar wind penetrates below

the altitude of 600 km). This evidence indicates that the majority of the electrons included within the electron peaks that are observed in the photoelectron spectrum discussed in this paper are most likely from carbon dioxide ionization rather than from atomic oxygen ionization; however, the fact that production of photoelectrons from atomic oxygen dominates over that from carbon dioxide at altitudes greater than about 200 km suggests that the fraction of photoelectrons between atomic oxygen and carbon dioxide changes with altitude. ELS does not possess the energy resolution required to distinguish between photoelectrons generated from photoionization of atomic oxygen and those generated from photoionization of carbon dioxide.

CO_2 is preferentially ionized by UV near the martian exobase where the atmosphere is dense and the CO_2 molecule has not dissociated. Due to the tenuous atmosphere of Mars, the ejected photoelectrons are transported along the local magnetic field lines. Some of the magnetic field lines have a component directed vertically with respect to the exobase surface. If both ends of the local magnetic field lines are connected to the planet, the local field traps the photoelectrons. At Mars, the field is due to remanent surface magnetization. In the ionosphere the photoelectrons are trapped within the local magnetic field and mirror inside the remanent magnetization fields or are lost to the atmosphere. Photoelectrons on open magnetic field lines can be scattered, reflected, or transported away from the ionosphere, depending on the shape of the field line. Away from the ionosphere on the nightside of the planet (at about two mars radii or greater) at altitudes just inside and near the IMB, the magnetic field lines are approximately parallel to the IMB (Liemohn et al., 2006) and show similar photoelectron signatures as in the martian ionosphere (photoelectrons mostly flowing away from the planet).

Our measurements in the martian upper ionosphere (Fig. 2) illustrate many of the characteristics of the photoelectrons. The color scale was chosen to emphasize the CO_2 photoelectron peaks and this choice displays the higher energy flux electrons as color saturated (red). The photoelectron peaks are quite stable and prominent in all 16 sectors comprising the ELS 360° FOV. Under oversampling conditions, there were two distinct photoelectron peaks (21–24 eV and 27 eV as determined by theory) which are easier to identify in the spectra shown in Fig. 3 than in the spectrogram of Fig. 2; the two photoelectron peaks are not always resolvable in survey mode as this depends on the sampling particulars.

At about 06:39 UT on June 7, 2004 (Figs. 1 and 2), the spacecraft observes sunrise and the photoelectrons appeared as the He 304 Å shone on the atmosphere and CO_2 photoelectrons were liberated. Between 06:50:30 and 06:55:30 UT, the photoelectron peaks became sporadic and were lost. Magnetosheath plasma was detected beginning at 06:55:30 UT. The photoelectron flux flowing from the planet is larger than the flux flowing toward to the planet. When the energy flux represented in the region of the CO_2 peaks is examined around the entrance plane (Fig. 4), one finds larger fluxes at the largest sector numbers and a seemingly discontinuous level between sector 0 and sector 1. The discontinuity between sector 0 and sector 1 is due to spacecraft influence.
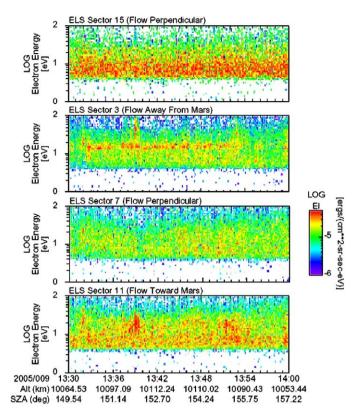
Fig. 7. Energy–time spectrogram in the martian tail. Values of differential energy intensity are color coded in the same format as Fig. 2. Spectrograms are marked with the electron flow direction. Photoelectron peaks are observed flowing away from the planet. The format of this plot is similar to that shown in Fig. 2.
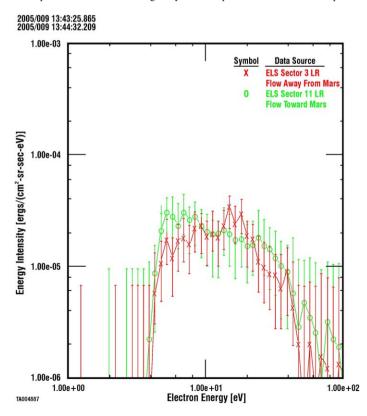

Fig. 8. Energy spectra of martian tail photoelectrons. The electron spectrum viewing approximately parallel to the IMB and toward the planet detecting electrons flowing away from Mars (red sector 3), and viewing away from the planet detecting electrons flowing toward Mars (green sector 11) are shown in a similar format to Fig. 3. Photoelectron peaks are shown flowing away, but not toward the planet. Error bars indicate average error values for 1 min and include Poisson statistics, instrument error, and telemetry compression error. Here, the solar latitude is $-27.0°$, solar time is 23.99 h, solar zenith angle is 153.2°, planetocentric longitude is 150.4°, planetocentric latitude is $-40.1°$, planetodetic latitude is $-40.2°$, and the planetodetic altitude is 10,113.4 km.
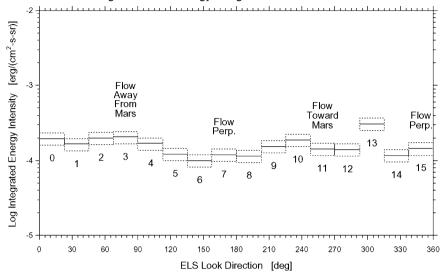
Fig. 9. ELS look directions of martian tail photoelectron intensities. ELS look directions around its viewing plane are shown as an integral of differential energy intensity including only the energy region of the CO_2 photoelectron peaks (shown in a similar format to Fig. 4). Electron flow directions are indicated.

When CO_2 photoelectron fluxes are remapped using a model magnetic field (Fig. 5), we see that the lower number sectors have lower fluxes than the higher number sectors. Interestingly, the averages of the intensities at pitch angles for the time interval represented in Fig. 3 are rather flat across the pitch angle range. Other cases of photoelectrons in the ionosphere closer to the subsolar point show that the photoelectron region was quite isotropic. Again, during the majority of times in the ionosphere, intensities in the photoelectron region for sectors which viewed across the spacecraft were greater than those which viewed into space, suggesting that the spacecraft influenced this population.

In the martian tail (Fig. 7), photoelectron peaks were observed only in ELS sectors which pointed toward the planet observing electrons flowing away from Mars, but not from the tail direction flowing toward Mars (Fig. 8), indicating that electron plasma from the dayside ionosphere was escaping the planet. In fact, the electron plasma returning from the tail showed a different characteristic, in that it displayed more bursts and covered a wider energy range (even extending above the energy range of the CO_2 peaks) as shown in sector 11. This suggests that the returning plasma is from a different source than the atmosphere.

A measurement angle analysis of tail electron plasma shows a sinusoidal variation (Fig. 9). When ELS sector directions were projected on the orbital plane shown in Fig. 6, sectors with the largest fluxes were found to be parallel to the average position of the IMB suggesting that the observed fluxes were flowing both toward and away from the planet, just inside of the IMB. Perpendicular fluxes were about a factor of 2 less than those flowing along the tail. If the magnetic field is parallel to the IMB in this region of the martian tail, this suggests a distribution flowing parallel to the magnetic field. Because of the spacecraft influence, it is unclear if there is a net current within

this region. However, in the region of the CO_2 photoelectron peaks, the flux within the peak region was slightly greater for electron distributions flowing away from the planet than flowing toward the planet.

A gyrotropic particle distribution which is flowing along a magnetic field with almost no flow perpendicular to the magnetic field is expected to produce a three-dimensional flux distribution which is cigar shaped, with the highest fluxes close to the direction of the magnetic field and the lowest fluxes perpendicular to the direction of the magnetic field. The detector cuts that cigar shape with a measurement plane located at some angle (other than 90°) with respect to the magnetic field. Viewing the flux in the plane of the detector, one expects a sinusoidal variation in azimuth around the plane, where the location of the largest flux values are the closest to the magnetic field direction and the smallest flux values are perpendicular to the magnetic field.

When observed in the tail of Mars, atmospheric photoelectron peaks were found near the IMB and have never been observed in the magnetosheath. Since tail observations have been shown to be highly directional, the observations are dependent on the specifics of the IMB crossing. Photoelectrons have also never been observed in the central tail or at locations very far from the IMB. This suggests that the photoelectrons are flowing away from the planet, parallel to the IMB, having been produced somewhere on the dayside of the planet. At the present time, the mechanism by which photoelectrons from the dayside ionosphere escape into the tail of Mars is not known. Among the possibilities are included the rearrangement of magnetic flux at the IMB on the dayside of the planet liberating photoelectrons to flow tailward, and magnetic field lines which are attached to the dayside of the planet and are stretched to form the tail conduit by which photoelectrons from the atmosphere can travel down the tail. One would think that liber-

ated electrons would escape the planet and not return; whereas, stretched dayside magnetic field lines imply closure and photoelectrons should be observed flowing toward the planet somewhere in the orbit (of course, there are also mechanisms which can empty flux tubes as geometry is important). The connection to electrons moving toward the planet is uncertain at this time.

Not all tail plasma which showed CO_2 peaks displayed a total flow directed away from the planet. In one case at 6000 km altitude (April 24, 2004, at 07:00:02 UT, with a planetodetic altitude of 7107.4 km, a solar zenith angle of 146.9°, a planetocentric latitude of 13.15°, and a planetocentric longitude of 242.65°), the returning photoelectrons were reduced by about 2 eV in energy relative to the peak energies flowing away from the planet. In this case, it appears as though the returning photoelectrons had begun cascading to lower energies. In most other cases, the spacecraft blocked the return flow and no separate peaks were observed. However in these cases, it is uncertain if the spacecraft generated photoelectrons influenced the detected plasma in the concerned ELS sectors or if there were just no CO_2 photoelectrons coming from the tail.

6. Conclusion

The electron spectrometer on Mars Express measures the differential electron spectrum over the range of 1 eV–20 keV from a 360° × 4° measurement plane divided into 16 sectors, each 22.5° wide and every 4 s. The energy resolution of 8% enables measurement of peaks in spectra identified with the excitation of atmospheric CO_2 with the following results.

The CO_2 peaks are easily observed on low-altitude cases (altitudes less than ~600 km) when Mars Express passes through the martian ionosphere. In the ionosphere, the CO_2 peaks are observed on the dayside on almost every orbit. The CO_2 photoelectron peaks are observed in all ELS sectors which can at times cover the entire pitch angle range. These peaks are shifted in energy compared to theoretical values due to a negative spacecraft potential which occurs in the ionosphere.

Photoelectron populations exhibiting the CO_2 peaks are also observed at greater altitudes and other local times. They are observed over the full range of Mars Express altitudes from periapsis of 250 km to an observation near apoapsis at 10,000 km. They are usually observed just interior to the inner boundary of the magnetosheath (the induced magnetosphere boundary of Lundin et al., 2004). In one case, the peaks at 6000 km show evidence of further interactions by being less well defined or degraded in energy.

The observation at the highest altitude (10,000 km) occurs on the nightside in the magnetotail. In this observation, the region of the photoelectron spectrum containing the peaks shows flow both toward and away from the planet. In the specific region of the CO_2 photoelectron peaks, the flux of electrons flowing away from the planet is greater and exhibits well defined peaks compared to the electron flux flowing toward the planet. Flux measured by sensors perpendicular to flow directions is significantly less. Liemohn et al. (2006) present results from an MHD and kinetic model of photoelectron production

and transport. Their results reproduce many of the features presented in this paper and give insight on the magnetic topology of Mars.

References

Barabash, S., and 46 colleagues, 2004. ASPERA-3: Analyzer of space plasmas and energetic ions for Mars Express. In: Wilson, A. (Ed.), Mars Express: A European Mission to the Red Planet. ESA SP-1240. ESA Publications Division, ESTEC, Noordwijk, The Netherlands, pp. 121–139.

Brain, D.A., Bagenal, F., Acuña, M.H., Connerney, J.E.P., 2003. Martian magnetic morphology: Contributions from the solar wind and crust. J. Geophys. Res. 108 (A12), 1–14, doi:10.1029/2002JA009482. SMP 8.

Cain, J.C., Ferguson, B.R., Mozzoni, D., 2003. An $n = 90$ internal potential function of the martian crustal magnetic field. J. Geophys. Res. 108, doi:10.1029/2000JE001487.

Connerney, J.E.P., Acuña, M.H., Wasilewski, P.J., Kletetschka, J., Ness, N.F., Réme, H., Lin, P.R., Mitchell, D.L., 2001. The global magnetic field of Mars and implications for crustal evolution. Geophys. Res. Lett. 28, 4015–4018.

Fox, J.L., Dalgarno, A., 1979. Ionization, luminosity, and heating of the upper atmosphere of Mars. J. Geophys. Res. 84, 7315–7333.

Johnstone, A.D., Alsop, C., Burge, S., Carter, P.J., Coates, A.J., Coker, A.J., Fazakerley, A.N., Grande, M., Gowen, R.A., Gurgiolo, C., Hancock, B.K., Narheim, B., Preece, A., Sheather, P.H., Winningham, J.D., Woodliffe, R.D., 1997. PEACE: A Plasma Electron and Current Experiment. Space Sci. Rev. 79, 351–398.

Krasnopolsky, V.A., Gladstone, G.R., 1996. Helium on Mars: EUVE and PHOBOS data and implications for Mars' evolution. J. Geophys. Res. 101, 15765–15772.

Liemohn, M.W., and 50 colleagues, 2006. Numerical interpretation of high-altitude photoelectron observations. Icarus 182, 383–395.

Lundin, R., and 44 colleagues, 2004. Solar wind-induced atmospheric erosion at Mars: First results from ASPERA-3 on Mars Express. Science 305, 1933–1936.

Mantas, G.P., Hanson, W.B., 1979. Photoelectron fluxes in the martian ionosphere. J. Geophys. Res. 84, 369–385.

Mitchell, D.L., Lin, R.P., Mazelle, C., Réme, H., Cloutier, P.H., Connerney, J.E.P., Acuña, M.H., Ness, N.F., 2001. Probing Mars' crustal magnetic field and ionosphere with the MGS Electron Reflectometer. J. Geophys. Res. 106, 23419–23427.

Sablik, M.J., Scherrer, J.R., Winningham, J.D., Frahm, R.A., Schrader, T., 1990. TFAS (a tophat for all species): Design and computer optimization of a new electrostatic analyzer. IEEE Trans. Geosci. Remote Sens. 28, 1034–1048.

Vignes, D., Mazelle, C., Rème, H., Acuña, M.H., Connerney, J.E.P., Lin, R.P., Mitchell, D.L., Cloutier, P., Crider, D.H., Ness, N.F., 2000. The solar wind interaction with Mars: Locations and shapes of the bow shock and the magnetic pile-up boundary from the observations of the MAG/ER experiment onboard Mars Global Surveyor. Geophys. Res. Lett. 27 (1), 49–52.